IET Journals
The Institution of Engineering and Technology

A Synchronous Reference Frame Interface for Geographically Distributed Real-Time Simulations

ISSN 1751-8644
doi: 0000000000
www.ietdl.org

Mazheruddin H. Syed[1], *Efren Guillo-Sansano*[1], *Steven M. Blair*[1], *Andreas Avras*[2], *and Graeme M. Burt*[1]

[1] *Institute for Energy and Environment, University of Strathlcyde, Glasgow, G1 1RD, UK*
[2] *Power Networks Demonstration Centre, University of Strathclyde, Glasgow, G68 0EF, UK*
* *E-mail: mazheruddin.syed@strath.ac.uk*

Abstract: The increasing complexity of power systems has warranted the development of geographically distributed real-time simulations (GD-RTS). However, the wide scale adoption of GD-RTS remains a challenge owing to the (i) limitations of state-of-the-art interfaces in reproducing faster dynamics and transients, (ii) lack of an approach to ensure a successful implementation within geographically separated research infrastructures, and (iii) lack of established evidence of its appropriateness for smart grid applications. To address the limitations in reproducing of faster dynamics and transients, this paper presents a synchronous reference frame interface for GD-RTS. By means of a comprehensive performance characterization (application agnostic and application oriented), the superior performance of the proposed interface in terms of accuracy (reduced error on average by 60% and faster settling times) and computational complexity has been established. This paper further derives the transfer function models for GD-RTS with interface characteristics for analytical stability analysis that ensure stable implementations avoiding the risks associated with multiple RI implementations. Finally, to establish confidence in the proposed interface and to investigate GD-RTS applicability for real-world applications, a GD-RTS implementation between two RIs at the University of Strathclyde is realized to demonstrate inertial support within transmission network model of the Great Britain power system.

1 Introduction

The transition of power system operation and control from a centralized to decentralized and distributed paradigm has brought forth challenges in validation and de-risking of novel solutions in support of their accelerated roll out and adoption. Recognizing the limitations of any single research infrastructure (RI) to support the transition, the concept of geographically distributed real-time simulations (GD-RTS) enables exploitation of the complementarity of diverse equipment, models and expertise to address the challenge [1–3]. With the first reported use of the term GD-RTS within the power systems context reported in 2006, deployments to date around the world span across continents - a transatlantic implementation [4], transpacific implementation [5] and a transoceanic link between Europe and Southeast Asia [6].

Technologically, advancements in GD-RTS have been realised on two fronts, improving the communications (comprising network, protocols, time delay determination and compensation) between the two RIs and enhancing the interface (comprising the interface algorithm , interface signals and corresponding transformation). As the information exchange between two geographically separated RIs is typically over the Internet, there is only minor enhancement to the network that can be made by the power system community. However, incremental advancements in protocols [7], time delay determination [8] and compensation [9] have been reported.

The interface algorithm defines the interconnection approach of the two subsystems of the GD-RTS. A number of interface algorithms have been described in the literature for power hardware-in-the-loop (PHIL) setups, as summarized in [10], and can be readily utilized for GD-RTS setups, owing to similar electrical subsystem division and real time operation. Through extensive experience gained from PHIL simulations, the ideal transformer method has established its dominance as the "go to" choice for GD-RTS interface algorithms given its straightforward implementation and good stability performance[11]. The use of instantaneous time domain representation of interface signals was shown to be inappropriate for GD-RTS due to the lack of an approach to compensate for the time delay and significant distortion introduced by time varying communications delays [12]. The interface signals are therefore transformed before their exchange over the Internet. To allow elimination of the effect of the time delay on the interface electrical waveforms, the exchange of interface signals in the form of Root Mean Square (RMS), frequency and phase angle was proposed in [13] and alternatively using Fourier coefficients (referred to as dynamic phasors) in [14]. Although the incorporation of phase information allowed for the effect of time delay to be compensated in the RMS approach, reduced fidelity for adequate reproduction of waveforms under dynamics and transients in comparison to that of phasors was highlighted in [15]. Phasor interface, currently acknowledged as the state-of-the-art, suffers from two shortcomings: (i) reduced speed of response, limiting faster transients reproduction (such as phase shifts) due to its windowing characteristic [14] and (ii) high computational complexity [7]. To address the challenge of increased computational complexity on resource constrained real-time simulators, an external FPGA node exclusively for phasor decomposition and exchange was discussed in [16]. However, this leads to additional costs (for FPGA node) and increased delays due to additional interface requirements (between the real-time simulator and FPGA node). As an alternative, a custom phasor decomposition model using moving average filter was developed for real-time simulators in [7]. However, this still encompasses reduced speed due to the windowing characteristics and the implementation has not been rigorously assessed.

Similar to PHIL setups, the stability analysis of GD-RTS configurations should be undertaken analytically to avoid risks of equipment damage (if involved) and to save time. The analysis of tthe stability of GD-RTS setups thus far reported has been time-domain simulation based [17] , presenting a risk where stability is assessed upon implementation and during run-time. Analytical stability assessment and the impact of interface transformations have not been taken into consideration. The interface transformation utilized can impact the stability of the GD-RTS, similar to the improvement when a filter is included in a PHIL simulation [11]. Therefore, the precise characteristics of interface transformation techniques needs to be incorporated

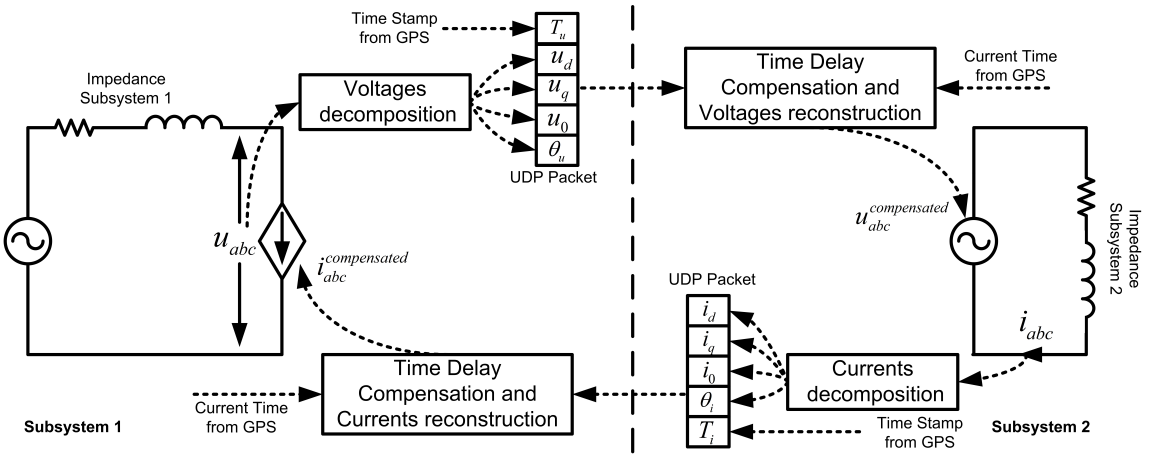

Fig. 1: Geographically separated real-time setup comprising two subsystems.

within stability analysis to optimally evaluate the use of the most appropriate interface for each scenario.

With the primary objective of GD-RTS to enable the capability to undertake high-fidelity large system validation studies, examples of synchronously coupled setups in literature have so far been limited to (i) small electrical circuits [4, 14] or (ii) setups where systems are split across a stronger grid (e.g. transmission grid) and weaker grid (e.g. distribution grid) [2, 15, 18]. Furthermore, applications have been limited to slower dynamics studies (such as voltage control) with some work on droop control reported in [19]. However, these examples do not provide a rigorous assessment of the applicability of the GD-RTS for smart grid applications that can enforce confidence in its wide-spread utilization.

Therefore, the contributions of this paper are two fold: (i) advancing the state-of-the-art and (ii) establishing the art-of-the-possible, as summarized below:

To address the shortcomings of the phasor interface, a novel synchronous reference frame interface is proposed. Although synchronous reference frame is an established transformation technique, its incorporation within the interface algorithm and the corresponding adaptations to enable GD-RTS presents novel knowledge applicable not only to GD-RTS setups but directly translatable to PHIL setups. Thorough comparative performance evaluation (application agnostic and application oriented) with the state-of-the-art phasor interface establishes its superior performance addressing the two shortcomings of the phasor interface dentified.

To enable accurate analytical stability assessment of GD-RTS setups, transfer function models of setups with phasor and synchronous reference frame interface have been derived. In a step-change from the state-of-the-art, the derived model allows for assessment of stability of a GD-RTS setup incorporating the impact of the transformation utilized. The stability analysis with derived model applied to a reference system has highlighted the following useful insights: (i) the use of a phasor interface inherently impacts the stability of a GD-RTS due to its windowing characteristics equivalence to a moving average filter, (ii) the proposed interface does not inherently impact the stability, however, when required allows for the stability of the setup to be enhanced by incorporation of a low pass filter (LPF) with high cut-off frequency ensuring minimal loss of speed of response and accuracy. This further demonstrates the value of the model derived that will help potential users of the GD-RTS approach to make an informed selection of interfaces and also demonstrates the additional flexibility of the proposed interface.

The applicability of the interface to enable large scale system studies has been established by two means: (i) demonstrating a complex system split where a larger transmission network is split into two synchronously coupled subsystems as opposed to the conventional approach of stronger grid - weaker grid coupling, and (ii) undertaking a rigorous assessment of a frequency control study to establish confidence in the fidelity offered by the interface.

The remainder of the paper is organized as follows. The proposed interface for GD-RTS setups is presented in Section 2, followed by a derivation of the transfer function model of phasor and synchronous reference interface for stability analysis in Section 3. A comprehensive application agnostic performance assessment of the proposed interface with the state-of-the-art phasor interface is presented in Section 4. Section 5 presents an application oriented performance characterization with GD-RTS implementation between two RI's at the University of Strathclyde, the Dynamic Power Systems Laboratory and the Power Networks Demonstration Centre, wherein the suitability of the proposed interface for frequency control within the transmission system of Great Britain (GB) is established. Section 6 concludes the paper.

2 Proposed Interface for GD-RTS

A single line diagram of the GD-RTS setup comprising two subsystems considered for this work is shown in Fig. 1 with the following subsections detailing the different components that are used for the interfacing of these subsystems.

2.1 Interface Algorithm

The interface algorithm defines the interconnection approach of the two subsystems of the GD-RTS. A number of interface algorithms have been described in the literature for PHIL setups, as summarized in [10], and can be readily utilized for GD-RTS setups, the reason being that these setups share the same electrical subsystem division and real time operation. For the purpose of this work, the voltage-type ideal transformer method (V-ITM) [20] where the voltage from subsystem 1 end is represented at the subsystem 2 end using a controlled voltage source, and the currents from the subsystem 2 end are fed back using a controlled current source at the subsystem 1 end (as shown in Fig. 1). This interface algorithm has been selected due to its straightforward implementation and good stability performance [11].

2.2 Interface Signals Decomposition

As is evident from the previous subsection, the choice of signals that are exchanged at the interface is determined by the interface algorithm chosen. For the given setup, the output interface signals from subsystem 1 are the three phase voltages while the three phase currents are the output interface signals from subsystem 2. As time domain signals have been proven to be unsuitable for direct transmission over packet-based communication [21], the instantaneous values of the interface signals need to be transformed. A requirement for choosing the transformation method for the interface signals of GD-RTS is the capability of time delay compensation, which

requires access to the phase of the signal [22]. The method chosen at one end dictates the choice of interface signal reconstruction at the other end. In this paper, Park's transformation ($dq0$), also referred to as synchronous reference frame transformation, is used for performing the signal decomposition.

The voltage direct component (u_d), quadrature component (u_q) and zero component (u_0) can be obtained from the instantaneous three phase voltages (u_a, u_b and u_c) using:

$$\begin{bmatrix} u_d \\ u_q \\ u_0 \end{bmatrix} = \frac{2}{3} \begin{bmatrix} cos(\omega t) & cos\left(\omega t - \frac{2\pi}{3}\right) & cos\left(\omega t + \frac{2\pi}{3}\right) \\ -sin(\omega t) & -sin\left(\omega t - \frac{2\pi}{3}\right) & -sin\left(\omega t + \frac{2\pi}{3}\right) \\ \frac{1}{2} & \frac{1}{2} & \frac{1}{2} \end{bmatrix} \begin{bmatrix} u_a \\ u_b \\ u_c \end{bmatrix} \tag{1}$$

In a similar manner the current direct component (i_d), quadrature component (i_q) and zero component (i_0) can be obtained from the instantaneous three phase currents (i_a, i_b and i_c):

$$\begin{bmatrix} i_d \\ i_q \\ i_0 \end{bmatrix} = \frac{2}{3} \begin{bmatrix} cos(\omega t) & cos\left(\omega t - \frac{2\pi}{3}\right) & cos\left(\omega t + \frac{2\pi}{3}\right) \\ -sin(\omega t) & -sin\left(\omega t - \frac{2\pi}{3}\right) & -sin\left(\omega t + \frac{2\pi}{3}\right) \\ \frac{1}{2} & \frac{1}{2} & \frac{1}{2} \end{bmatrix} \begin{bmatrix} i_a \\ i_b \\ i_c \end{bmatrix} \tag{2}$$

2.3 Communications Protocol and Time Synchronization

The GD-RTS interface setup requires the exchange of information from one subsystem to the other, and an appropriate communications protocol and technology are required to be chosen. User datagram protocol (UDP) has been selected as the communications protocol to be implemented due to its suitability for real-time applications [23]. The interface signals from each subsystem are packed into a UDP packet and transferred to the other subsystem. As shown in Fig. 1, subsystem 1 has five output interface signals, voltage dq0 components (u_d, u_q and u_0 respectively), the phase of the voltage (θ_u), and the time stamp (T_u). Similarly, the output interface signals of subsystem 2 are the current dq0 components (i_d, i_q and i_0 respectively), phase of the current (θ_i) and the time stamp (T_i). As the two subsystems are geographically separated, the exchange of information can be completed via a number of technologies over the internet. The technologies (for example, ethernet, fiber, LTE, etc.) involved will depend upon the available communications infrastructure interlinking the two subsystems.

The communication of the interface signals between the two subsystems introduces delay that for the purpose of accuracy and stability needs to be compensated. Accurate time delay compensation requires of an accurate measurement of the time delay [8]. For GD-RTS, the only feasible option is to implement a time synchronization method, either using public network time protocol (NTP) over internet or global positioning system (GPS). A public NTP would be an economical option, however the accuracy would depend upon the reliability of the internet connection and the frequency at which a ping for synchronization can be obtained. For reliable operation, GPS time synchronization becomes imperative, requiring a GPS clock at either end of the GS-RTS setup.

For the setup under consideration, a GPS-based time synchronization is utilized. The interface signals at each end (subsystem 1 and subsystem 2) are time stamped before being sent as part of the exchanged signals over the interface.

2.4 Time Delay Compensation and Interface Signals Reconstruction

Time delay is calculated at each subsystem end upon receipt of the UDP packet by means of subtracting the time stamp of the UDP packet from the current GPS time. The time it takes for the UDP packet to reach from subsystem 1 to subsystem 2 is referred to as the feed-forward time delay $\tau_{d_{ff}}$ and the time taken for UDP

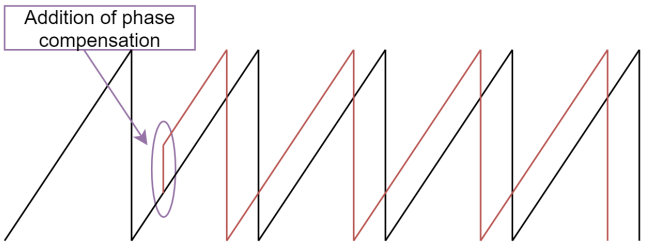

Fig. 2: Phase compensation on instantaneous phase signal.

packet to reach from subsystem 2 to subsystem 1 is referred to as feedback time delay $\tau_{d_{fb}}$. The feed-forward time delay advances the reconstructed voltage at subsystem 2 in reference to the voltage at subsystem 1 by a phase equivalent to the measured time delay calculated as

$$\varphi_{ff} = \tau_{d_{ff}} \cdot 2 \cdot \pi \cdot f_h \tag{3}$$

where the frequency f_h is the nominal frequency of each harmonic component to be compensated. Similarly, the feedback time delay advances the reconstructed current waveform at subsystem 1 in reference to the current at subsystem 2 by a phase equivalent to the measured time delay calculated as

$$\varphi_{fb} = \tau_{d_{fb}} \cdot 2 \cdot \pi \cdot f_h \tag{4}$$

The impact of time delay can be compensated while reconstructing the waveform at each subsystem end by means of shifting the measured phase signal [9]. In this manner, the shifted waveform will be equal to the ideal, non-delayed waveform. For an accurate compensation, the feed-forward and feedback phase compensation term (φ_{ff} and φ_{fb}), need to be adaptive to frequency, this is illustrated as:

$$\begin{aligned} \varphi_{ff} &= \tau_{d_{ff}} \cdot 2 \cdot \pi \cdot f_{h_m} \\ \varphi_{fb} &= \tau_{d_{fb}} \cdot 2 \cdot \pi \cdot f_{h_m} \end{aligned} \tag{5}$$

where the frequency f_{h_m} is the measured frequency of each harmonic component under consideration rather than a fixed nominal frequency. Using fixed nominal frequency results in steady-state errors following any transient. The interface signals are reconstructed using inverse Park's transformation as:

$$\begin{bmatrix} u_a \\ u_b \\ u_c \end{bmatrix} = \begin{bmatrix} cos(\omega t + \varphi_{ff}) & -sin(\omega t + \varphi_{ff}) & 1 \\ cos\left(\omega t - \frac{2\pi}{3} + \varphi_{ff}\right) & -sin\left(\omega t - \frac{2\pi}{3} + \varphi_{ff}\right) & 1 \\ cos\left(\omega t + \frac{2\pi}{3} + \varphi_{ff}\right) & -sin\left(\omega t + \frac{2\pi}{3} + \varphi_{ff}\right) & 1 \end{bmatrix} \begin{bmatrix} u_d \\ u_q \\ u_0 \end{bmatrix} \tag{6}$$

$$\begin{bmatrix} i_a \\ i_b \\ i_c \end{bmatrix} = \begin{bmatrix} cos(\omega t + \varphi_{fb}) & -sin(\omega t + \varphi_{fb}) & 1 \\ cos\left(\omega t - \frac{2\pi}{3} + \varphi_{fb}\right) & -sin\left(\omega t - \frac{2\pi}{3} + \varphi_{fb}\right) & 1 \\ cos\left(\omega t + \frac{2\pi}{3} + \varphi_{fb}\right) & -sin\left(\omega t + \frac{2\pi}{3} + \varphi_{fb}\right) & 1 \end{bmatrix} \begin{bmatrix} i_d \\ i_q \\ i_0 \end{bmatrix} \tag{7}$$

3 Stability Analysis of GD-RTS

In this section, the transfer function models of GD-RTS setups with phasor and synchronous reference frame interface for stability analysis are derived and consequently utilized for a comparative stability assessment of the proposed interface to that of a phasor interface.

The single input single output (SISO) representation of the GD-RTS setup is presented in Fig. 3a and its open-loop transfer function

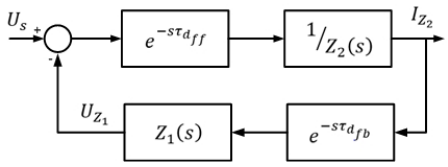

(a) SISO representation of GD-RTS setup.

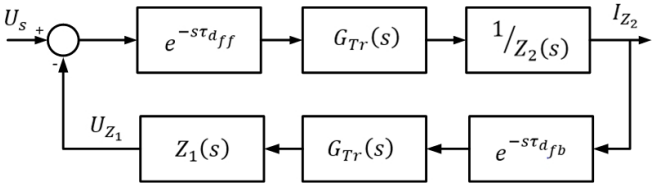

(b) Representation of GD-RTS incorporating transformation transfer function.

Fig. 3: Representation of GD-RTS setups.

is defined by

$$F_O(s) = \frac{Z_1(s)e^{-s\cdot T_d}}{Z_2(s)} \tag{8}$$

where $Z_1(s)$ and $Z_2(s)$ are the series connected equivalent impedances of subsystem 1 and subsystem 2 respectively. The time delay T_d is the sum of the feed-forward and feedback delay represented as

$$T_d = \tau_{d_{ff}} + \tau_{d_{fb}} \tag{9}$$

Similar to the stability assessment of PHIL setups, the stability of the GD-RTS setups can be evaluated with the Nyquist stability criterion [24, 25]. The assessment requires the determination of poles of the closed-loop system equivalent to the zeros of the following two characteristic equations [26]

$$1 + F_O(s) = 0 \tag{10}$$

$$det(\mathbf{I} + \mathbf{F}_O(s)) = 0 \tag{11}$$

where $\mathbf{I}$ is the appropriate dimension identity matrix. Incorporating the transfer function of the transformation, represented as $G_{Tr}(s)$, within the feed-forward and feedback loop of GD-RTS as shown in Fig. 3b, the open-loop transfer function can be represented as

$$F_O(s) = \frac{Z_1(s)G_{Tr_{ff}}(s)G_{Tr_{fb}}(s)e^{-s\cdot T_d}}{Z_2(s)} \tag{12}$$

where the suffixes $_{ff}$ and $_{fb}$ represent the transfer function in feed-forward loop and feedback loop respectively. The windowing characteristic of a discrete Fourier Transform (DFT) can be approximated as a moving average filter, represented in continuous domain as

$$G_{DFT}(s) = \frac{1}{T_w}\left(\frac{1}{s} - \frac{e^{-T_w s}}{s}\right) = \frac{1 - e^{-T_w s}}{T_w s} \tag{13}$$

where T_w is the length of the window. The frequency shifting property of the Fourier transform shifts the input signal by $-f_h$ upon decomposition and by f_h during reconstruction. This shifting in frequency does not impact the signal itself, however, its impact on the approximated windowing characteristic $G_{DFT}(s)$ should be taken into consideration for stability assessment. The frequency shifting property can be represented as

$$x(t) \Leftrightarrow X(s) \tag{14}$$

$$x(t)e^{s_0 t} \Leftrightarrow X(s - s_0) \tag{15}$$

where, for the case under consideration,

$$s_0 = j2\pi f_h \tag{16}$$

where f_h is the frequency of the h^{th} harmonic under consideration. The transfer function of the DFT with reconstruction can therefore be defined as

$$G_{DFT_R}(s) = \frac{1}{(s - s_0)T_w}\left(1 - e^{-(s-s_0)T_w}\right) \tag{17}$$

The analysis so far only considers the fundamental component, however, if stability with multiple harmonic components is to be analyzed with parallel DFT functions, the representative transfer function is then described by the sum of each component transfer function as

$$G_{DFT_{R_h}}(s) = \sum_{h=1,\dots,N} \frac{1}{(s - s_0)T_w}\left(1 - e^{-(s-s_0)T_w}\right) \tag{18}$$

Similar to DFT, the Park's transformation $dq0$ also exhibits the frequency shifting property. No filtering is applied to the fundamental component when utilizing the transform, with LPFs employed for harmonic transformation. The transfer function can be therefore represented by

$$G_{dq0_{R_h}}(s) = \sum_{h=1,\dots,N} \frac{1}{1 + (s - s_0)T_{w_{ch}}} \cdot e^{s_0 T_d} \tag{19}$$

where w_{ch} represents the corresponding harmonic cut-off frequency. The GD-RTS open-loop transfer function with DFT can therefore be represented as:

$$F_O(s) = \frac{Z_1(s)G_{DFT_{R_{h_{ff}}}}(s)G_{DFT_{R_{h_{fb}}}}(s)e^{-s\cdot T_d}}{Z_2(s)} \tag{20}$$

and with $dq0$ as:

$$F_O(s) = \frac{Z_1(s)G_{dq0_{R_{h_{ff}}}}(s)G_{dq0_{R_{h_{fb}}}}(s)e^{-s\cdot T_d}}{Z_2(s)} \tag{21}$$

Table 1 System values for Nyquist assessment

Subsystem 1 (Z_1)	$R_1 = 1.2\,\Omega$	$L_1 = 3\,$mH
Subsystem 2 (Z_2)	$R_2 = 1\,\Omega$	$L_2 = 2\,$mH
Other	$T_w = 0.02\,$s	$T_d = 600\,\mu$s

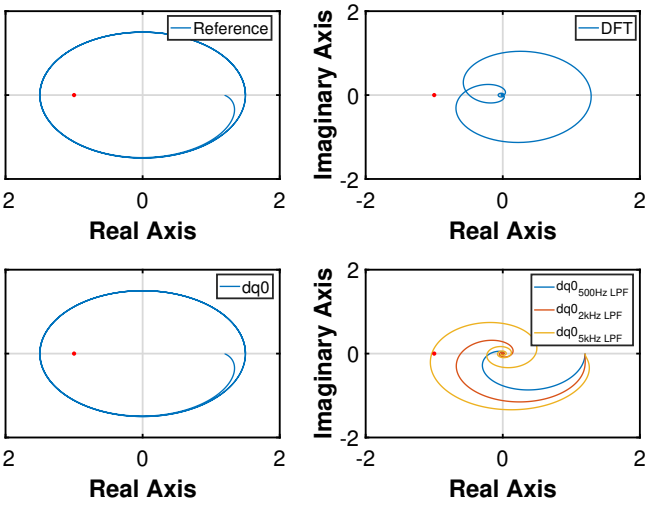

Fig. 4: GD-RTS stability assessment.

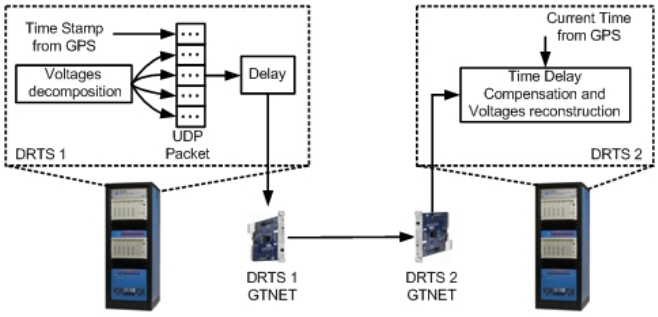

(a) Application agnostic performance characterization setup.

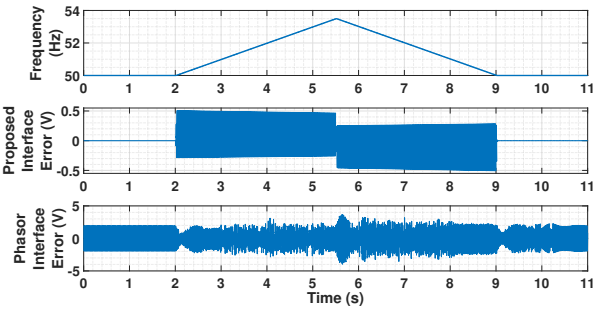

(b) Dynamic response.

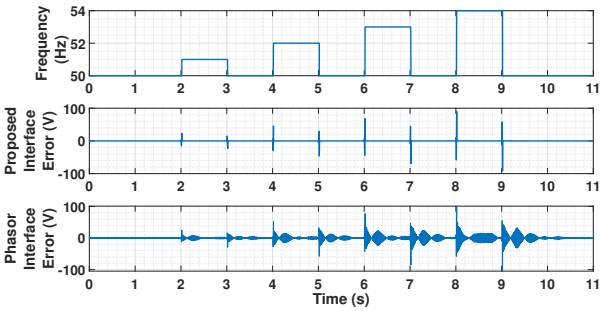

(c) Transient reproduction.

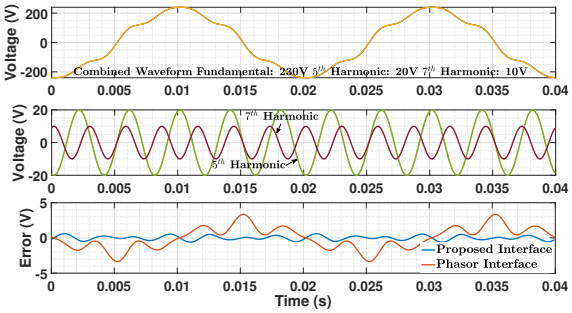

(d) Harmonics reproduction.

Fig. 5: Application agnostic performance characterization setup and analysis.

With the GD-RTS transfer function representations at hand, the stability is analyzed on an example GD-RTS system such as that of Fig. 1. The parameters of the system are presented in Table 1 and the results of the analysis are shown in Fig. 4. The system without any transformation is referred to as the reference system and as can be observed from Fig. 4 (top left) is unstable with the chosen parameters. The use of synchronous reference frame interface does not impact the stability of the system as is evident from Fig. 4 (bottom left). On the other hand, the use of phasor interface improves the stability of the system (Fig. 4 top left). Typically, the use of a transformation should not impact the stability of a system, however, this improvement in stability is due to the DFT windowing characteristic equivalence to a moving average filter. The typical use of a one cycle window length for a DFT, even though it improves the stability of the system, the dynamic and transient response are negatively impacted as has been demonstrated in Section 4.1. The proposed synchronous reference frame interface enables the use of a more traditional approach to improve the system stability, that is the incorporation of a LPF on the feedback path of the system. The assessment of stability of the system with the proposed interface incorporating a feedback path LPF is presented in Fig. 4 (bottom left). The incorporation of a relatively high cut-off frequency LPF (2kHz) provides stability improvement similar to that of the phasor interface with much faster response under dynamic and transient events.

4 Application Agnostic Performance Characterization of Proposed Interface

In the literature, the use of phasors for transmission of interface signals over packet-based communications has been consistently reported, with claimed benefits of improvement in fidelity and stability [12, 15, 17]. As described in Section 2.2 and 2.4, the proposed interface utilizes Park's transformation for decomposition /reconstruction rather than phasor decomposition /reconstruction using DFT as in a phasor interface. This section presents an application agnostic comparison of a phasor interface with the proposed interface for the sole purpose of geographically distributed simulations. The setup for application agnostic comparison of the two methods is shown in Fig. 5a, where two digital real-time simulators (DRTS) from RTDS Technologies are utilized with the simulated model run at a time step of 50 μs. This involves the decomposition of a three-phase signal (voltage waveform in this case) in DRTS 1, transmission over a local network using UDP (sent out of DRTS 1 to DRTS 2) with a static delay of 16 ms and its reconstruction using the same method with time-delay compensation in DRTS 2. As the signal being decomposed and reconstructed is sinusoidal, the metric used for comparison is the instantaneous error calculated as

$$\epsilon = V_N - V_R \tag{22}$$

where V_N is the reference waveform while V_R is the reconstructed waveform. The following sub-sections report the comparison in detail.

4.1 Steady State, Dynamic and Transient Performance

In this subsection, the performance of the two methods in steady state condition, response to dynamic and transient events is compared. Here, steady state refers to the condition when there is no change in frequency, dynamic event refers to a change in frequency over seconds, whereas a change in frequency over milliseconds is attributed to a transient event.

The results of the comparison for phase a of the three-phase signal are shown in Fig. 5b and 5c. As can be observed, for $dq0$ the steady state error is $\sim$0 V and for a dynamic event the error is less than 0.5 V. In comparison, the phasor interface presents a continuous error in steady state of up to 2 V and a varying error up to 4 V during the dynamic event. From Fig. 5c, it can be observed that the instantaneous error upon sudden change in frequency is relatively high for both the proposed and phasor interface. However, the error for the proposed interface returns to a steady state value much faster than the phasor interface. The error for the phasor interface returns to steady state, however with an increase in the magnitude of the transient, it takes a longer time for the error to return to the steady state value. From the above, it can be said that the decomposition and reconstruction method using the proposed interface presents better steady state accuracy, better dynamic response and faster transient response compared to a method that utilizes a phasor interface.

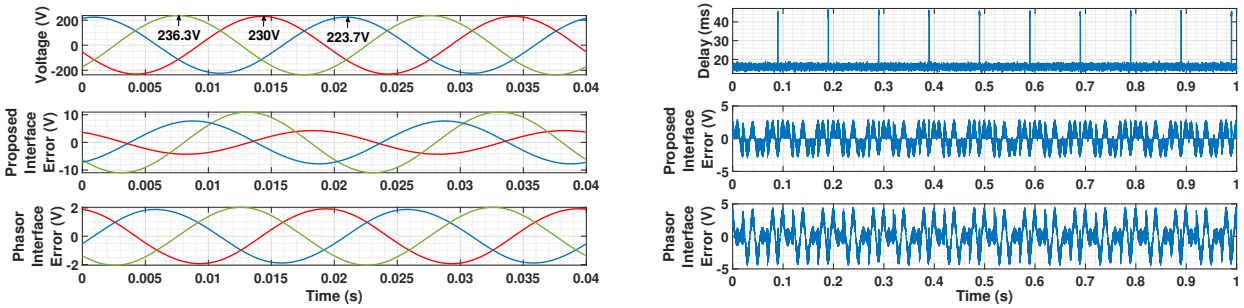

(a) Imbalance reproduction.

(b) Response under variable communications delay.

Fig. 6: Application agnostic performance characterization analysis.

In the above implementation, the ωt utilized for two interfaces is the same, however the DFT is much more sensitive to changes in frequency. This behaviour of a phasor interface has also been verified in another commercial power systems simulator (MATLAB) where the accuracy of DFT for signal reconstruction deteriorates at off nominal frequencies. Custom implementations of DFT algorithms with additional signal processing can render superior performance.

4.2 Performance under presence of Harmonics

In this subsection, the performance of the two methods for accurate reproduction of a waveform with harmonics is discussed. Any individual harmonic component can be extracted using the proposed interface with the use of appropriate LPFs [27]. A waveform comprising a fundamental of magnitude 230 V, 5^{th} harmonic of magnitude 20 V and 7^{th} harmonic of magnitude 10 V is used as a reference. The results are shown in Fig. 5d. As can be observed, the accuracy of the proposed interface is improved in comparison with the accuracy of the phasor interface. It is worth mentioning that the reproduction of harmonics using DFT is limited to the 8^{th} harmonic within the DRTS utilized here, while no such limitation exists when using $dq0$.

4.3 Performance under Unbalance

In this subsection the performance of the two methods for accurate reproduction of three-phase waveform with imbalance is discussed. A three-phase waveform with 230 V, 236.3 V and 223.7 V as respective phase magnitudes is used as reference as shown in Fig. 6a. These magnitudes have been chosen as per ANSI C.841 standard that defines a design and operational limit for an electrical supply system to maximum voltage imbalance of 3 %. It is known that the performance of $dq0$ under imbalance is not appropriate but as can be observed from Fig. 6a, the error is limited to 10 V.

4.4 Performance under Variable Communications Delay

In the previous subsections, the performance characterization is undertaken with a static delay of 16ms. This subsection discusses the performance of the two approaches under variable communications delay.

Communications delays between RIs in Europe are stable given their interconnectivity through GÉANT - the pan-European data network for the research and education community [28]. GÉANT interconnects 19 European countries with data link speeds in magnitude of multiples of 100 Gbps, extended Europe with link speeds in magnitude of multiples of 10 Gbps, and wider continental Europe with links of 1-9 Gbps. A topology map can be found in [29]. A similar network exists within the USA, referred to as the Energy Sciences Network (ESnet) supported by the Department of Energy [30] and is connected to GÉANT via the transatlantic fibre link between the continents [31].

However, owing to the non-deterministic nature of the communications delays, the impact of random communications delays on the performance of the two approaches is shown in Fig. 6b. The delay profile is a summation of the static delay, Gaussian noise (mean=0.016, standard deviation=0.005) and random value as in Fig. 6b (top). As can be observed from the results, the performance of the two approaches is not significantly impacted by the sudden random spike in communications delay, however the proposed interface yields superior performance in comparison to the phasor interface.

Table 2 Computational complexity

	dq0	DFT
Decomposition Function	$abc/dq0$ 4.3 μs	n-sample DFT 3*(0.18*n+0.5) μs
Reconstruction Function	$dq0/abc$ 4.25 μs	sin 3* 1.3 μs
Total	8.55 μs	0.54*n+5.4 μs

4.5 Computational Complexity

In this subsection, the computational complexity of the two methods is compared. Many components utilized for decomposition and reconstruction are common for the two methods, for example the phase locked loop to acquire the ωt, therefore, only the computational complexity of the components unique to the methods are presented in Table 2. The method utilizing Park's transformation requires one function for decomposition ($abc/dq0$) and one for reconstruction ($dq0/abc$) with a total computational time of 8.55 μs on the target DRTS processor. The method utilizing DFT requires three functions for deconstruction (one DFT for each phase) and three for reconstruction (one sin function for each phase). The computational time of the DFT is a function of n, i.e. the number of samples per cycle acquired for calculation. The DRTS utilized offers a maximum of $n = 64$, leading to a total computational time of 39.96 μs. As is evident, the method utilising DFT is $\sim$ 4.5 times computationally more expensive than the method utilizing $dq0$. This calculation presented is for the fundamental component only, the complexity increases linearly with an increase in the number of harmonics. Recursive DFT or sliding DFT methods offer improved computational performance, however their performance has not been compared to that of $dq0$ due to their unavailability within the simulation tools utilized.

5 Application Oriented Performance Characterization: GD-RTS for Frequency Control

5.1 GD-RTS Setup

5.1.1 Geographically Separated Research Infrastructures: The GD-RTS experimental setup is shown in Fig. 7a. Two RIs at the University of Strathclyde have been utilized: (i) Dynamic Power Systems Laboratory (DPSL) is a 100kW microgrid facility

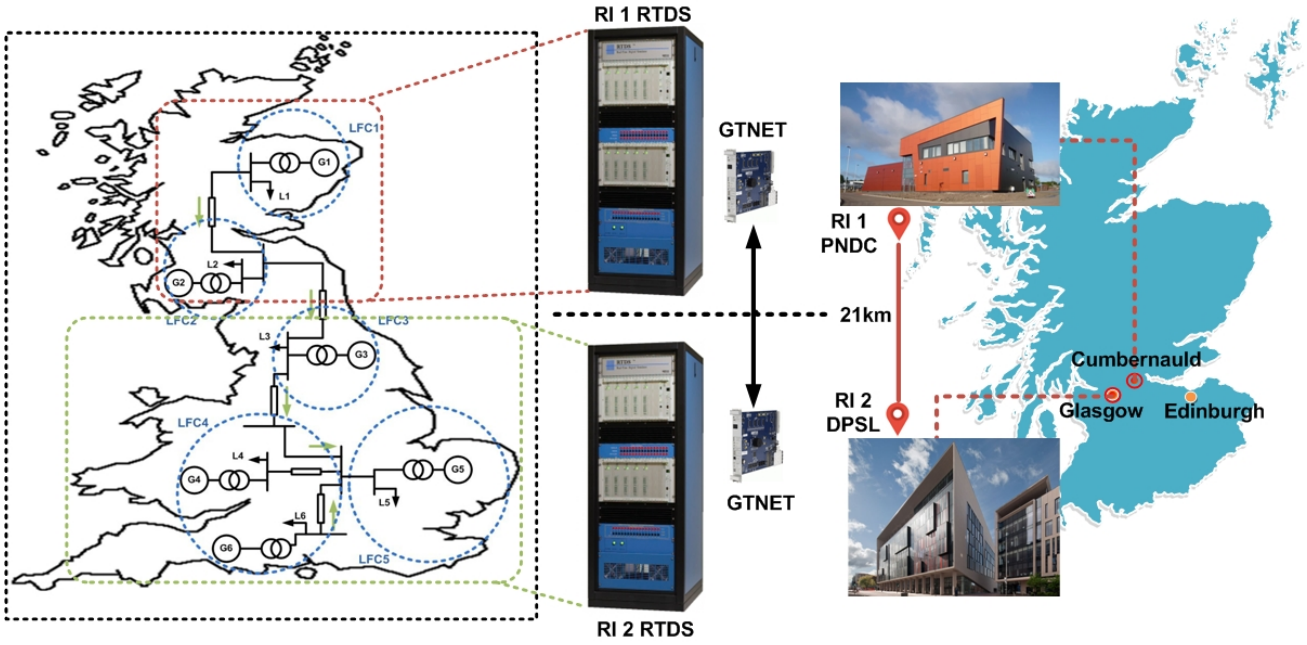

(a) Geographically distributed real-time laboratory setup.

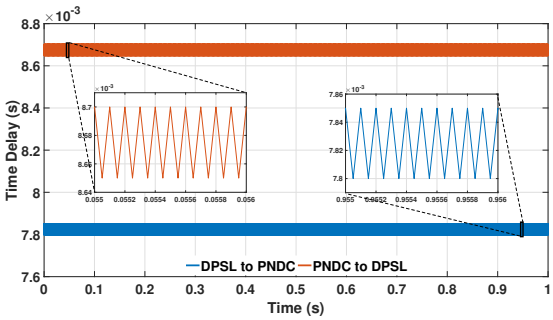

(b) Time delay of the setup.

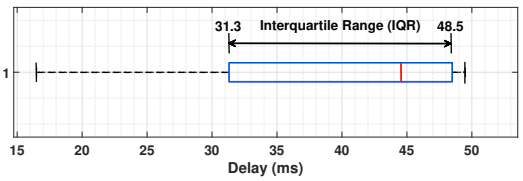

(c) Interquartile range for delays presented in Table 3.

Fig. 7: Distributed real-time laboratory setup at University of Strathclyde between the two research infrastructures, PNDC and DPSL.

housed at the Technology and Innovation Centre within the Glasgow City Innovation District, in the centre of the city of Glasgow; (ii) Power Networks Demonstration Centre (PNDC) is a MW scale industry facing experimental facility located at Cumbernauld, 21km north-east of Glasgow. The coordinates and postcodes of the two RIs are presented in Table 3. For the purpose of real-time simulations, one DRTS at each RI is employed communicating over public communications infrastructure via the GTNET communications cards.

5.1.2 Power system model: To demonstrate the suitability of the GD-RTS with the proposed interface for real-world smart grid applications, a reduced eight-bus dynamic model of the GB power system has been chosen as the test grid. The GB grid is a single synchronous area and has no load frequency control (LFC) areas. However, in this paper, buses of the reduced model have been grouped to represent LFC areas as shown in Fig. 7a. These regions have been developed around major generation sources, power flow corridors and load centers [32]. The model has been developed in RSCAD and simulated in real-time at a time-step of 50μs using a digital real-time simulator from RTDS Technologies, with each area comprising at least one aggregated generator and an aggregated load. The model has been validated by means of two tests, a load flow analysis and a dynamic frequency response evaluation, in [33]. The tuning of the governor during the dynamic response validation of the test grid yielded a droop value of 13 %. Other model parameters can be found in [34], and hence have not been repeated in this paper.

For the purpose of GD-RTS, the reduced dynamic model of the GB power system has been split in two, as shown in Fig. 7a. Two of the five LFC areas are simulated within RTDS at RI-1 (PNDC) and the remaining three LFC areas are simulated within RTDS at RI-2 (DPSL). The split model is interfaced via the V-ITM interface algorithm with the controlled voltage source at RI-1 and the controlled current source at RI-2. The split model connected over the ITM IA presents a challenge in terms of its initialization and synchronization, where the network in RI-2 cannot initialize without the presence of the remainder of the network (being simulated at RI-1), as reported in [35]. The process recommended for such setups in [35] is adopted to allow for successful initialization and synchronization before any further evaluation is undertaken.

Table 3 Geographic information of the two research infrastructures

Research Infrastructure	Latitude	Longitude	Postcode
RI 1 PNDC	55.972219	-3.972405	G68 0EF
RI 2 Dynamic Power	55.860664	-4.242896	G1 1RD

5.1.3 Interface communications setup: The interface signals between the two RIs are exchanged at the maximum allowed rate, i.e., 10kHz, limited by the GTNET (digital communication input/output) cards utilized. The feed-forward loop time delay of the given setup can be defined as the time it takes for the interface signals to reach from RI-2 to RI-1 while the feedback loop time delay is defined as the time it takes for the interface signals to reach from

Table 4 Analyzing time delay within Europe

City	Country	Average Ping Delay (ms)	Jitter (ms)	Payload (ms)	Total Delay (ms)
London	UK	12.6	0.7	6	19.3
Paris	France	18.5	0.5	6	25
Frankfurt	Germany	24.9	0.4	6	31.3
Stockholm	Sweden	37.5	0.6	6	44.1
Zurich	Switzerland	35.5	0.6	6	42.1
Bratislava	Slovakia	37.8	1.2	6	45
Milan	Italy	35.8	0.9	6	42.7
Sevilla	Spain	42.7	0.5	6	49.2
Vienna	Austria	38.9	0.4	6	45.3
Warsaw	Poland	41.6	0.8	6	48.4
Brno	Czechia	42.2	0.3	6	48.5
Budapest	Hungary	42.2	1.1	6	49.3
Belgrade	Serbia	42.8	0.7	6	49.5

RI-1 to RI-2. The feed-forward and the feedback loop delays of the given setup are shown in Fig. 7b. The time delay of any setup that involves more than one fixed time-step simulator is often varying, as the signal from the first fixed-step simulator will have to wait till the next time-step of the second fixed time-step simulator (unless the two simulators are perfectly synchronized, which is not often the case) [8]. In the given setup, the two fixed-step simulators are the real time simulators at either end (one RTDS at DPSL and one RTDS at PNDC), as a consequence of which in both the feed-forward and the feedback delay, a variation of 50 μs exists. The sum of the feedback and feed-forward delay is equal to $\sim$ 16.5 ms and will be referred to as the inherent delay (ID) of the setup, with the setup itself referred as Distributed D1.

Given the near proximity of the two RIs, the delay exhibited by the setup is quite modest. To analyze the delay, a simple ping test between the two RIs was conducted resulting in a delay of 11.5 ms (round trip). Although the distance between the two RIs is small, with a fibre link present between the two infrastructures, the relatively larger 11.5ms delay is associated to the firewalls within the network. The additional $\sim$ 6 ms (D1-11.5 = 6 ms) round trip delay is associated to the payload of the message being exchanged. As identified earlier, due to the stable fibre link between the two RIs, only a relatively small 100 μs (round trip) jitter also exists within the delay. As the work in this paper is undertaken as part of the European Commision's H2020 ERIGRID project, where the objective is to interconnect RIs within Europe, ping tests from RI-2 to a number of cities within Europe were undertaken, results of which are presented in Table 4. To allow for investigation of setups within the European context, the interquartile range (IQR) for the set of delays is calculated (as shown in Fig. 7c) and the 25^{th} and 75^{th} percentile values are obtained as 31.3 ms and 48.5 ms respectively. Two additional cases are considered, the first case involves addition of 8 ms of static delay to both feed-forward path and feedback path in addition to the inherent delay and the setup is referred to as Distributed D2. The second case involves addition of 16 ms of static delay to both feed-forward and feedback path in addition to the inherent delay and the setup is referred to as Distributed D3. The delays of setup Distributed D2 and Distributed D3 represent the 25^{th} and 75^{th} percentile approximately.

5.2 *Application to Frequency Control*

In this section, the applicability of distributed setups to study frequency control is assessed. Power system frequency control refers to the process of maintaining equilibrium between the generation and load in steady state, while restoring the equilibrium following a disturbance with as little unintentional load loss as possible [36], and is the responsibility of the system operator. Frequency control can be broadly classified in four stages based on the timescale of its operation: (i) inertial response up to 10 seconds from the initiation of the disturbance, (ii) primary frequency control, response from first few seconds up to 30 seconds, (iii) secondary frequency control, response from 30 seconds to 30 minutes and (iv) tertiary frequency control, from 15 minutes up to several hours. In the following subsections, the frequency response of the GD-RTS systems is characterized against a monolithic setup (i.e. without GD-RTS) followed by a case-study to further assess the applicability and role of GD-RTS.

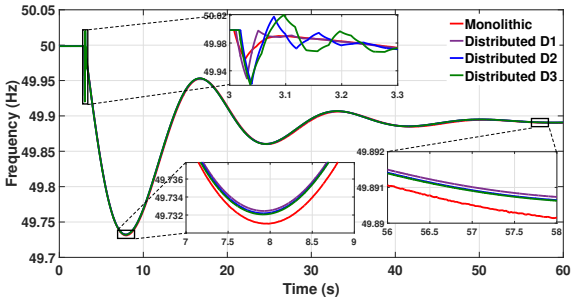

(a) Frequency.

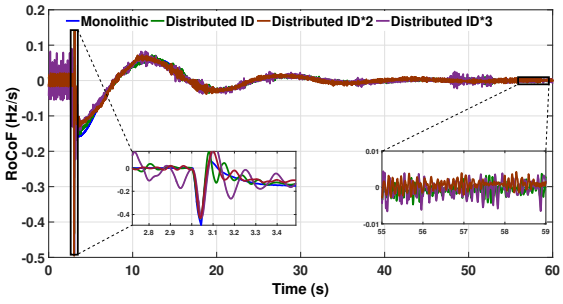

(b) RoCoF.

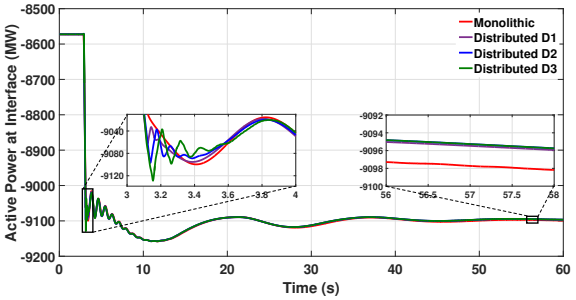

(c) Active power.

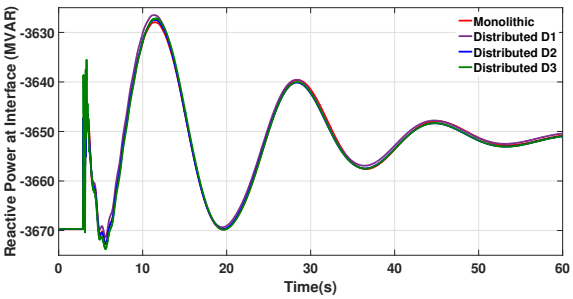

(d) Reactive power.

Fig. 8: System response to 1000MW generation loss , comparing monolithic and GD-RTS studies with the proposed interface.

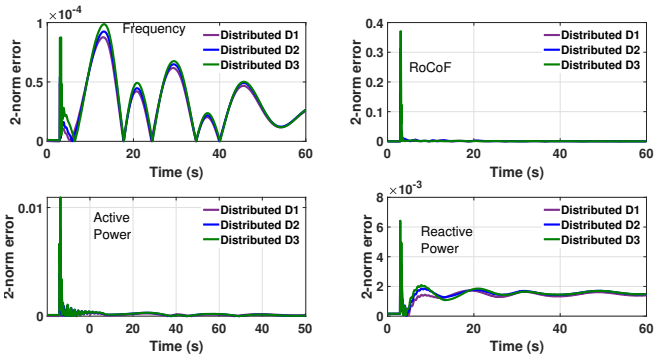

(a) 2-norm error using proposed interface.

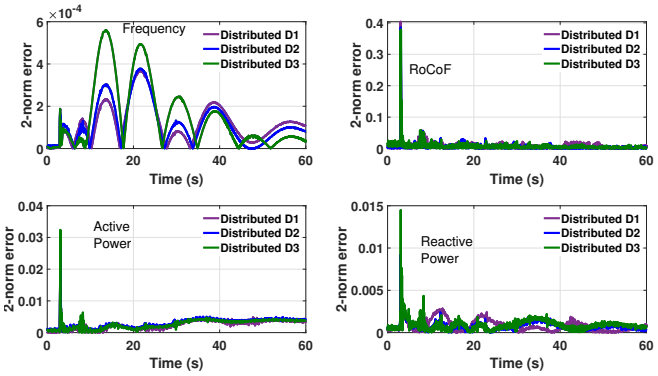

(b) 2-norm error using phasor interface.

Fig. 9: 2-norm error for four parameters under consideration.

5.2.1 Characterization: For the purpose of characterizing the system frequency response, a 1000MW step increase in load emulating a generation loss is initiated within LFC 4. Four system parameters are characterized: (i) frequency: the frequency is measured using a zero crossing detection method. One measurement per LFC area is obtained and the average of the 5 areas characterized, (ii) the rate of change of frequency (RoCoF): one measurement per area, measured over a time period of $T = 20$ms, averaged for the five areas, (iii) active power: the active power exchange at the interface/point of common coupling (PCC), and (iv) reactive power: the reactive power exchange at the interface/PCC. The system response subject to 1000MW generation loss is presented in Fig. 8, with system frequency in Fig. 8a, RoCoF in Fig. 8b, the active and reactive power in Fig. 8c, and Fig. 8d respectively. As can be observed from the figures, the performance of the distributed setup with the proposed interface is in close agreement with the results obtained through a monolithic setup. To more effectively characterize the difference, a fidelity metric using 2-norm is defined as

$$M_2 = \frac{\|x - x_r\|_2}{\|x_r\|_2} \tag{23}$$

where, x is the value of parameter under consideration measured for distributed setup, x_r is the reference value of the parameter under consideration measured for monolithic setup. The error is calculated over a one cycle period. The normalization of the relative error with reference quantity provides a more realistic comparison of system parameters, specifically of different scales. The 2-norm error for the four parameters for the study are shown in Fig. 9a. The least error is observed for frequency of the system while the highest error for the RoCoF. It is important to note that the relatively high error in RoCoF is measured within the first 300ms after the event. This blip in measurement of RoCoF is well documented [37] and is associated to the phase step of the voltage rather than the RoCoF itself. Without considering the first 300ms of RoCoF, the maximum 2-norm error can be calculated as 0.0058, 0.0061 and 0.0063 for Distributed D1, D2 and D3 respectively. In other words it can be said that the use of distributed setup for calculation of voltage phase offset subject to a disturbance yields large errors and might be unsuitable in applications that utilize phase offset as in [38].

To benchmark the performance of the proposed interface against the phasor interface, the 2-norm errors for the four parameters using the phasor interface are shown in Fig. 9b. The maximum 2-norm errors for the four parameters are summarized in Table 5. The errors follow a similar trend for the two interfaces, they increase with increasing time delay, are minimum for frequency and maximimum for RoCoF. With the complex interactions of two strongly coupled subsystems, the superior performance of the proposed interface over the phasor interface are evident, with significant improvement in accuracy offered for all the four parameters characterized with an average reduction of the peak error in the different parameters of approximately 60%.

5.2.2 Case Study: The fastest control requirement is for inertial response, where response is desired immediately after an event. Therefore, if a simulation setup is suitable for inertial response, it can be said that the same setup is suitable for primary, secondary and tertiary frequency control. For this reason, this sub-section evaluates the applicability of real-time distributed simulation setup for inertial response.

The control under consideration is the swing equation based inertial response (SEBIR) as reported in [39]. SEBIR control is considered to be a potential solution to allow for power electronic interfaced generation or load to support the system during and after disturbances. As the name suggests, the principle of operation of SEBIR is based on the swing equation, as shown in equation (14)

$$\Delta P = \frac{2H}{f_{nom}} \frac{df}{dt} \tag{24}$$

where ΔP is the magnitude of power imbalance in the system, H is the inertia constant of the area under consideration, f_{nom} is the nominal frequency of the system. Upon occurrence of an event that leads to power imbalance in the system, e.g. for a loss of a generator, the system frequency drops resulting in a negative RoCoF. The SEBIR control implementation is shown in Fig. 10a. As can be observed, based on the RoCoF, additional active power response from participating resources is provided to support the frequency of the network.

To assess the applicability of the distributed setup for inertial response, SEBIR control is incorporated within the five-areas of the GB power system. It is assumed that 20% of the system load is flexible and interfaced by means of power electronics, counting towards the inertial response contributing devices within the network. The RoCoF is calculated over a period of 20ms representing the delay as

Table 5 Characterization through 2-norm for frequency control.

Parameter	Distributed D1		Distributed D2		Distributed D3	
	Proposed Interface	Phasor Interface	Proposed Interface	Phasor Interface	Proposed Interface	Phasor Interface
Frequency	8.744×10^{-5}	3.6810×10^{-4}	9.2287×10^{-5}	3.7809×10^{-4}	9.8429×10^{-5}	5.5933×10^{-4}
RoCoF	0.2356	0.3792	0.3090	0.3859	0.3795	0.4038
Active Power	0.0064	0.0259	0.0088	0.0280	0.0118	0.0324
Reactive Power	0.0017	0.0050	0.0026	0.0092	0.0042	0.0145

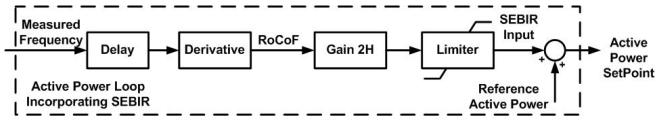

(a) SEBIR control implementation.

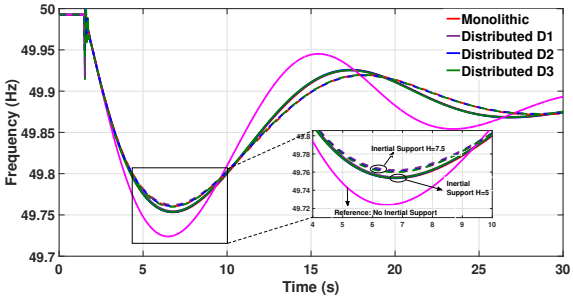

(b) A comparative frequency response.

Fig. 10: Applicability for inertial response, the control considered and results obtained.

depicted in Fig. 10a. Three cases are analyzed, (i) a reference case with no inertial support, (ii) inertial support with $H = 5$s and (iii) inertial support with $H = 7.5$s. The limiter is a rate limiter applied to improve the dynamics under inertial response chosen as 30MW/s in each of the areas.

The frequency responses of the four setups (monolithic, distributed D1, D2 and D3) for the two cases, $H = 5$s (solid lines) and $H = 7.5$s (dashed lines), are shown in Fig. 10b compared with the monolithic setup reference response (pink line). With the incorporation of inertial support, i.e., enabling additional active power support from participating resources within the network, the fall in frequency is alleviated and the nadir is improved. By increasing the inertia value from $H = 5$s to $H = 7.5$s, a minor improvement is observed, however, in practice the value of inertia constant that can be utilized is limited by the additional active power reserved/stored within the network. From the results presented, it is clear that the performance of the three distributed setups is within a close margin and within the error margin obtained for the characterization presented in earlier sub-section. It can therefore be said that the use of GD-RTS setups is applicable for study of inertial control and thereby to any consequent frequency control measure.

6 Conclusions

One of the challenges we face in facilitating the transition towards the future paradigm of decentralized and distributed power system operation is the limitations in accurately representing large system complexity and proving scalability for systems level validation of novel smart grid solutions, this paper therefore presents a synchronous reference interface for further advancing the capabilities of a key enabling concept - geographically distributed real-time simulations. A thorough comparative performance evaluation of the proposed interface against the current state-of-the-art phasor interface has been undertaken. Application agnostic comparison has demonstrated the superiority of the proposed interface under steady state, dynamic and transient events, in reproducing harmonics with selective time delay compensation, and under variable communications delay. In all the above cases, the proposed interface presents faster and improved response with minimal errors in comparison to the phasor interface. Furthermore, the proposed interface is computationally around 4.5 times faster than the phasor interface. A limitation of the proposed interface is its inability to reproduce imbalance conditions appropriately. However, the use of single phase synchronous reference frame transformation, specifically designed for individual phase reproduction, has not been explored.

The paper presents an example implementation of GD-RTS setup between two remote RIs at the University of Strathclyde. The setup is utilized for frequency control within the transmission network model of the Great Britain power system, serving for application oriented performance characterization of the proposed interface with the phasor interface. The proposed interface offers significant improvement in accuracy for all four parameters characterized. Having established its superior performance and the close proximity to the results compared with a monolithic setup, its use for swing equation based inertial response has been demonstrated. This is the first implementation example where a synchronous transmission network has been split across geographically distributed RIs for simulation, in contrast to implementations in literature where the split is between a stronger and a weaker network, typically transmission-distribution split or where a HVDC link separates the transmission network.

To support successful implementations and wider adoption of the GD-RTS approach with confidence, the transfer function model of GD-RTS setups with interface transformation characteristics has been derived for analytical stability assessment. Stability assessment of a reference setup with a phasor and the proposed interface has been undertaken revealing that the phasor interface impacts the stability of the setups due to its windowing characteristics, while the proposed interface does not inherently impact the stability of the system. The proposed interface offers a flexible approach where stability can be improved where required by means of a low pass filter with minimal loss in response speed.

The following two areas have been identified as future work: (i) the expansion of the proposed interface to incorporate controller and power equipment within a synchronously coupled controller and power hardware-in-the-loop setup distributed across multiple RIs, and (ii) pushing the boundaries of GD-RTS simulation to explore its use for analysis of back-up protection with the aid of phasor measurement units and wide-area monitoring and control.

Acknowledgments

This work was supported in part by the European Commission under the H2020 Programme's ERIGRID and ERIGRID2.0 projects (grant no: 654113 and 870620). The work has also been in part supported by the Nokia Energy Innovation Center, Plano, Texas, USA. Any opinions, findings and conclusions or recommendations expressed in this material are those of the authors and do not necessarily reflect those of the European Commission.

7 References

1 Mirz, M., Vogel, S., Schäfer, B., Monti, A. 'Distributed real-time co-simulation as a service'. In: 2018 IEEE International Conference on Industrial Electronics for Sustainable Energy Systems (IESES). (, 2018. pp. 534–539

2 Bompard, E., Monti, A., Tenconi, A., Estebsari, A., Huang, T., Pons, E., et al. 'A multi-site real-time co-simulation platform for the testing of control strategies of distributed storage and v2g in distribution networks'. In: 2016 18th European Conference on Power Electronics and Applications (EPE'16 ECCE Europe). (, 2016. pp. 1–9

3 Stevic, M., Vogel, S., Grigull, M., Monti, A., Estebsari, A., Pons, E., et al. 'Virtual integration of laboratories over long distance for real-time co-simulation of power systems'. In: IECON 2016 - 42nd Annual Conference of the IEEE Industrial Electronics Society. (, 2016. pp. 6717–6721

4 Stevic, M., Monti, A., Benigni, A. 'Development of a simulator-to-simulator interface for geographically distributed simulation of power systems in real time'. In: IECON 2015 - 41st Annual Conference of the IEEE Industrial Electronics Society. (, 2015. pp. 005020–005025

5 Lundstrom, B., et al.: 'Trans-oceanic remote power hardware-in-the-loop: multi-site hardware, integrated controller, and electric network co-simulation', *IET Generation, Transmission Distribution*, 2017, **11**, (18), pp. 4688–4701

6 Wang, Y., et al.: 'A distributed control scheme of microgrids in energy internet and its multi-site implementation', *IEEE Transactions on Industrial Informatics*, 2020, **66**, (1), pp. 1–1

7 Vogel, S., et al. 'Improvements to the co-simulation interface for geographically distributed real-time simulation'. In: IECON 2019 - 45th Annual Conference of the IEEE Industrial Electronics Society. vol. 1. (, 2019. pp. 6655–6662

8 Guillo-Sansano, E., Syed, M., Roscoe, A.J., Burt, G., Coffele, F.: 'Characterization of time delay in power hardware in the loop setups', *IEEE Transactions on Industrial Electronics*, 2020, pp. 1–1

9 Guillo.Sansano, E., Roscoe, A.J., Burt, G.M. 'Harmonic-by-harmonic time delay compensation method for phil simulation of low impedance power systems'.

In: 2015 International Symposium on Smart Electric Distribution Systems and Technologies (EDST). (, 2015. pp. 560–565
10 Brandl, R.: 'Operational range of several interface algorithms for different power hardware-in-the-loop setups', *Energies*, 2017, **10**, (12), pp. 1946. Available from: http://dx.doi.org/10.3390/en10121946
11 Ren, W., Sloderbeck, M., Steurer, M., Dinavahi, V., Noda, T., Filizadeh, S., et al.: 'Interfacing issues in real-time digital simulators', *IEEE Transactions on Power Delivery*, 2011, **26**, (2), pp. 1221–1230
12 Stevic, M., Estebsari, A., Vogel, S., Pons, E., Bompard, E., Masera, M., et al.: 'Multi-site european framework for real-time co-simulation of power systems', *IET Generation, Transmission Distribution*, 2017, **11**, (17), pp. 4126–4135
13 Liu, R., Mohanpurkar, M., Panwar, M., Hovsapian, R., Srivastava, A., Suryanarayanan, S.: 'Geographically distributed real-time digital simulations using linear prediction', *International Journal of Electrical Power Energy Systems*, 2017, **84**, pp. 308 – 317. Available from: http://www.sciencedirect.com/science/article/pii/S0142061516308079
14 Stevic, M., Vogel, S., Monti, A., D'Arco, S. 'Feasibility of geographically distributed real-time simulation of hvdc system interconnected with ac networks'. In: 2015 IEEE Eindhoven PowerTech. (, 2015. pp. 1–5
15 Stevic, M., Panwar, M., Mohanpurkar, M., Hovsapian, R., Monti, A. 'Empirical study of simulation fidelity in geographically distributed real-time simulations'. In: 2017 North American Power Symposium (NAPS). (, 2017. pp. 1–6
16 Vogel, S. 'Development of a modular and fully-digital PCIe-based interface to Real-Time Digital Simulator'. RWTH Aachen University, 2017
17 Stevic, M., Monti, A. 'A bilateral teleoperation approach for interface algorithms in distributed real-time simulations'. In: 2018 IEEE Workshop on Complexity in Engineering (COMPENG). (, 2018. pp. 1–5
18 Stevic, M., Vogel, S., Monti, A. 'From monolithic to geographically distributed simulation of hvdc systems'. In: 2018 IEEE 19th Workshop on Control and Modeling for Power Electronics (COMPEL). (, 2018. pp. 1–5
19 Vogel, S., Stevic, M., Kadavil, R., Mohanpurkar, M., Koralewicz, P., Gevorgian, V., et al. 'Distributed real-time simulation and its applications to wind energy research'. In: 2018 IEEE International Conference on Probabilistic Methods Applied to Power Systems (PMAPS). (, 2018. pp. 1–6
20 Ren, W., Steurer, M., Baldwin, T.L.: 'Improve the stability and the accuracy of power hardware-in-the-loop simulation by selecting appropriate interface algorithms', *IEEE Transactions on Industry Applications*, 2008, **44**, (4), pp. 1286–1294
21 Stevic, M., Estebsari, A., Vogel, S., Pons, E., Bompard, E., Masera, M., et al.: 'Multi-site european framework for real-time co-simulation of power systems', *IET Generation, Transmission Distribution*, 2017, **11**, (17), pp. 4126–4135
22 Guillo.Sansano, E.: 'Novel methods for enhancing accuracy and stability of power hardware-in-the-loop simulations'. (University of Strathclyde, 2018)
23 Tibor, S., Dukán, P., Odadžíc, B., Péter, O. 'Realization of reliable high speed data transfer over udp with continuous storage'. In: 2010 11th International Symposium on Computational Intelligence and Informatics (CINTI). (, 2010. pp. 307–310
24 Omar Faruque, M.D., Strasser, T., Lauss, G., Jalili-Marandi, V., Forsyth, P., Dufour, C., et al.: 'Real-time simulation technologies for power systems design, testing, and analysis', *IEEE Power and Energy Technology Systems Journal*, 2015, **2**, (2), pp. 63–73
25 Sastry, S.: 'Nonlinear Systems, Analysis, Stability and Control'. (Springer, 1999). Available from: https://www.springer.com/gp/book/9780387985138
26 Lauss, G., Strunz, K.: 'Multirate partitioning interface for enhanced stability of power hardware-in-the-loop real-time simulation', *IEEE Transactions on Industrial Electronics*, 2019, **66**, (1), pp. 595–605
27 Asiminoael, L., Blaabjerg, F., Hansen, S.: 'Detection is key - Harmonic detection methods for active power filter applications', *IEEE Industry Applications Magazine*, 2007, **13**, (4), pp. 22–33
28 GÉANT. 'GÉANT — at the heart of research and education networking'. (, . Available from: https://www.geant.org/About
29 GÉANT. 'GÉANT topology map'. (, . Available from: https://www.geant.org/Networks/Pan-European_network/Pages/GEANT_topology_map.aspx
30 ESnet. 'About ESnet'. (, . Available from: https://www.es.net/about/
31 ESnet. 'ESnet Map'. (, . Available from: https://www.es.net/assets/About-ESnet/15-CS-1035-ESnet-EuropeUS-MapEEXv4.pdf
32 'Electricity Ten Year Statement 2016",'. (National Grid, 2016). Available from: http://www2.nationalgrid.com/UK/Industry-information/Future-of-Energy/Electricity-ten-year-statement
33 Emhemed, A., Adam, G., Hong, Q., Burt, G. 'Studies of dynamic interactions in hybrid ac-dc grid under different fault conditions using real time digital simulation'. In: 13th IET International Conference on AC and DC Power Transmission (ACDC 2017). (, 2017. pp. 1–5
34 Syed, M.H.: 'Enhanced Frequency Control for Greater Decentralisation and Distributed Operation of Power Systems: Design to Laboratory Validation'. (University of Strathclyde, 2018)
35 Guillo.Sansano, E., Syed, M.H., Roscoe, A.J., Burt, G.M.: 'Initialization and synchronization of power hardware-in-the-loop simulations: A great britain network case study', *Energies 2018*, 2018, **11**, (5), pp. 1087
36 Kundur, P., Paserba, J., Ajjarapu, V., Andersson, G., Bose, A., Canizares, C., et al.: 'Definition and classification of power system stability ieee/cigre joint task force on stability terms and definitions', *IEEE Transactions on Power Systems*, 2004, **19**, (3), pp. 1387–1401
37 Wright, P.S., Davis, P.N., Johnstone, K., Rietveld, G., Roscoe, A.J.: 'Field measurement of frequency and rocof in the presence of phase steps', *IEEE Transactions on Instrumentation and Measurement*, 2019, **68**, (6), pp. 1688–1695
38 Syed, M.H., Guillo.Sansano, E., Blair, S.M., Roscoe, A.J., Burt, G.M.: 'A novel decentralized responsibilizing primary frequency control', *IEEE Transactions on Power Systems*, 2018, **33**, (3), pp. 3199–3201
39 Yu, M., Dysko, A., Roscoe, A., Booth, C., Ierna, R., Urdal, H., et al. 'Effects of swing equation-based inertial response (sebir) control on penetration limits of non-synchronous generation in the gb power system'. In: International Conference on Renewable Power Generation (RPG 2015). (, 2015. pp. 1–6